Energy Conversion and Management 323 (2025) 119264

Contents lists available at ScienceDirect

Energy Conversion and Management

journal homepage: www.elsevier.com/locate/enconman

Comparison of diesel and hydrotreated vegetable oil as the high-reactivity fuel in reactivity-controlled compression ignition

Jacek Hunicz [a,b], Liping Yang [b], Arkadiusz Rybak [a], Shuaizhuang Ji [b], Michał S. Gęca [a], Maciej Mikulski [c,*]

[a] Lublin University of Technology, Faculty of Mechanical Engineering, Nadbystrzycka 36, 20-618 Lublin, Poland
[b] Harbin Engineering University, College of Power and Energy Engineering, Nantong 145, 150001 Harbin, China
[c] University of Vaasa, School of Technology and Innovation, Efficient Powertrain Solutions (EPS), Wolffintie 34, FI-65200 Vaasa, Finland

ARTICLE INFO

Keywords:
RCCI
HVO
Natural gas
Fuel reactivity
Engine calibration

ABSTRACT

Hydrotreated vegetable oil (HVO) is becoming a widely accepted renewable drop-in alternative fuel to diesel. However, conventional diesel combustion does not fully exploit HVO's superior physicochemical parameters. Its high cetane index should significantly improve the performance and emission of next-generation, dual-fuel, reactivity-controlled compression ignition (RCCI) engines. These have a promising future in marine and off-road sectors. This study is the first comprehensive verification of HVO's benefits towards achieving superior RCCI combustion with natural gas. It used a sophisticated, single-cylinder research engine with a fully controllable air/fuel paths, calibrated in conventional compression ignition mode. The calibration experiments in a corresponding RCCI setpoint covered the cross-sensitivity of high-reactivity fuels (HVO and diesel) to boost pressure, excess air ratio, exhaust gas recirculation and start of injection, investigated at 85 % and 93 % energy-based blending ratios with natural gas. Extensive measurement instrumentation provided combustion and emission characterisation, enabling observations regarding both the phenomenology and applied potential of HVO-activated RCCI. Best performance was observed at the boundary of mixture dilution, restricted by the misfire or combustion variability limits. High reactivity of HVO allows for extending combustion stability limits, enabling increasing both, the local dilution (earlier injection timings) and the global dilution (higher mixture strengths or higher exhaust recirculation ratios). Calibrated along these phenomenological outcomes, HVO and diesel allow achieving efficiency over 2 percentage points superior in RCCI mode, compared to conventional diesel reference. With HVO, RCCI can be calibrated to comfortably meet EPA Tier 4 emission limits in all legislated species, without aftertreatment. Particular merits are in NO_X reduction, for which the best case HVO-RCCI tested at 0.7 g/kWh vs 2.8 g/kWh of diesel-RCCI. HVO further cuts down methane slip by more than 45 %, while PM emissions for RCCI are generally measured ultra-low. Corresponding conventional diesel reference exceeds the EPA NO_X and PM limits by respectively 1500 % and 400 %.

1. Introduction

Concerns about energy shortage, air pollution and greenhouse gases (GHG) have driven the electrification of passenger cars. However, reciprocating engines will occupy a dominant position in heavy trucks, agricultural machinery, construction equipment and ships because these engines provide high-power density, robustness and strong fuel adaptability [1,2]. The last of these characteristics is in high demand as zero and low-carbon fuels from different supply streams are needed to satisfy GHG reduction strategies in these sectors. Fuel flexibility has to be secured while maximising overall fuel efficiency and minimising the need for exhaust after-treatment [3,4].

Recent decades have seen much research into advanced premixed low-temperature combustion (LTC) concepts, such as homogeneous charge compression ignition (HCCI), premixed charge compression ignition (PCCI) and reactivity-controlled compression ignition (RCCI). They aim to promote engine efficiency and break the trade-off between oxides of nitrogen (NO_X) and soot emissions in diesel engines. These concepts can operate on variety of fuel combinations, with minimal hardware changes. Low combustion temperature of a highly diluted mixture inhibits the thermal NO_X formation pathways. Simultaneously,

* Corresponding author.
E-mail address: maciej.mikulski@uwasa.fi (M. Mikulski).

https://doi.org/10.1016/j.enconman.2024.119264
Received 15 September 2024; Received in revised form 9 November 2024; Accepted 9 November 2024
Available online 15 November 2024

Nomenclature

BR	Blend ratio
bTDC	Before top dead centre
CO	Carbon monoxide
CN	Cetane number
CTL	Coal-to-liquid
CR	Compression ratio
CDC	Conventional diesel combustion
COV-IMEP	Covariance of IMEP
CAD	Crank angle degree
CA05	CAD at 5 % fuel mass fraction burnt
CA50	CAD at 50 % fuel mass fraction burnt
CHR	Cumulative heat release
DF	Diesel fuel
EGR	Exhaust gas recirculation
FAME	Fatty acid methyl esters
FTIR	Fourier transform infrared
GHG	Greenhouse gas
HRR	Heat release rate
HRF	High reactivity fuel
HC	Hydrocarbons
HCCI	Homogeneous charge compression ignition
HVO	Hydrotreated vegetable oil
OH	Hydroxyl
IMEP	Indicated mean effective pressure
ITE	Indicated thermal efficiency
LRF	Low reactivity fuel
LHV	Lower heating value
LTC	Low-temperature combustion
MAP	Manifold absolute pressure
NG	Natural gas
NRMM	Non-road mobile machinery
NO_X	Oxides of nitrogen
PM	Particulate matter
PN	Particulate number
PODE	Polyoxymethylene dimethyl ethers
PCCI	Premixed charge compression ignition
PRR	Pressure rise rate
RCCI	Reactivity-controlled compression ignition
SOI	Start of injection
TDC	Top dead centre
VVA	Variable valve actuation
λ	Excess air ratio

longer mixing time and therefore a more homogeneous air–fuel mixture, can effectively reduce the proportion of diffusion combustion, allowing for control of soot emission [5]. But this combustion control is not straightforward because ignition and combustion onsets are determined indirectly by fuel reactivity or thermal stratification [6]. The dual-fuel concept of RCCI excels over the mentioned LTCs as combustion can be controlled in a fast, cycle-by-cycle manner by changing the blend ratio (BR) between high- and low-reactivity fuels (further referred to as HRF and LRF respectively). When combined with slower thermal management strategies, like charge-air temperature, external exhaust gas recirculation (EGR) or variable valve actuation, efficient fuel-flexible RCCI can be achieved across a wider range of engine loads than with HCCI or PCCI. NO_X and soot emissions can be simultaneously controlled, while obtaining thermal efficiency as high as 56 % in gross indicated thermal efficiency (ITE) at an indicated mean effective pressure (IMEP) up to 9.3 bar [3,5].

In the first RCCI experiments, Kokjohn et al. [7] used gasoline as LRF and automotive-grade diesel fuel (DF) as HRF. The experiments aimed to independently stratify fuel reactivity, equivalence ratio and temperature. The results showed that the reactivity gradient has a dominant effect on RCCI combustion, followed by the air–fuel ratio layer. The authors reported that the temperature stratification effect was an order of magnitude lower, and thus negligible. The study's main takeaway is that increasing the reactivity gradient between the fuels can improve the engine's thermal efficiency, extend the combustion boundary and reduce emissions.

Another studies by the same group focused on RCCI with natural gas (NG) as LRF [8,9]. NG has significantly lower reactivity than gasoline, while providing larger flammability limits and higher knock resistance (octane value of 120–130 for NG vs. 95 for gasoline). Fossil NG also has abundant availability compared to petroleum, while offering an intrinsic advantage of 25 % lower carbon footprint. Its GHG impact can be further reduced by complementing the supply chains with bio or electro-methane [10]. Yousefi et al. [8,9], positively verified the thesis that a larger reactivity gradient in diesel-NG RCCI is conducive to controlling the pressure rise rate. This enabled raising the high-load limit by 40 % compared to gasoline RCCI, while keeping the same low-NO_X emission footprint. Sacrificing this load extension, NG's large knock resistance allows a high compression ratio, so the thermal efficiency in dual-fuel engines can be comparable to diesel engines, but coupled with simultaneously reduced NO_X, sulphur oxides and particulate matter (PM) emissions [9].

Nieman et al. [11] pushed the above-mentioned limits of NG-diesel RCCI even further. They used combustion optimisation to keep PM and NO_X below Euro VI limits for heavy-duty trucks, while maintaining diesel-like load range. The authors further reported lower combustion noise. However, carbon oxide (CO) and unburned hydrocarbons (HC) emissions were very high, especially under low-load conditions.

The mechanisms behind the poor combustion efficiency of RCCI at partial loads were fundamentally investigated by Dronniou et al. [12]. They used a single-cylinder, optical research engine and recorded the single-cycle OH* chemiluminescence imaging using an enhanced charge-coupled device camera. This revealed that when the concentration of gas and air mixture is higher than the thin flammability limit, turbulent flame propagation can be observed in the gas-air mixture zone without diesel. However, when the mixture concentration is thinner than the combustible flammability limit, it cannot support flame propagation initialised by diesel fuel, thus resulting in large amounts of unburned methane emissions. Complementing these observations, numerical studies by Li et al. [13] and Yang et al. [14] showed that the pilot fuel combustion influences methane combustion under low engine loads, and that these processes are partially decoupled. The movement of the pilot's hot combustion products, into the methane-air mixture, controls the overall process. Excessive unburned hydrocarbon emission of dual-fuel engines mainly is caused by the cylinder mixture being too lean to support flame propagation: the contribution of clearance and liner boundary layer to methane emission is relatively small [13].

There are several ways to extend the RCCI load range by adding additional control parameters. They include thermal management by external hot EGR [15], LRF stratification by means of high-pressure direct injection of NG [16], variable compression ratio (CR) [17] or variable valve actuation (VVA) [18]. Of all these options, VVA is now been considered an enabler for next generation LTC engines, because, with a single piece of hardware, it can achieve a variety of control measures on a fast, in-cycle basis. Possible strategies for RCCI high-load extension typically involve early intake valve closing for apparent CR reduction to mitigate peak pressure rise rate (PRR) [19]. Low-load efficiency can be improved by increasing in-cylinder temperature with internal EGR [20]. Notably, exhaust gas recompression can be used to reform a portion of directly injected fuel, enabling a promising

alternative for on-board mixture reactivity adjustment [21]. Readers are referred to the latest work of Kim et al. for a comprehensive review of VVA strategies, including these applicable for RCCI, [22].

It is evident from the proceeding paragraphs that a route for applicable natural-gas RCCI is at hand. The above statement has been recently substantiated by Zhang et al. [23], reporting first tests of RCCI-adapted Wärtsilä 8 V31 DF marine engine in real-world sea trials. The tests prove that RCCI with DF and NG can reduce methane slip by 50 % compared to market-best gas engines, enabling a radical change in marine propulsion. Exploring full potential of this technology, however will be accompanied by increased system complexity and calibration challenges [24,25]. Furthermore, all the measures discussed above to increase the load range will be limited by the governing fuel reactivity span inherent in the diesel-natural gas principle of RCCI. Therefore, adjusting the fuel reactivity remains the primary measure to secure superior performance for RCCI. This explains why many studies have departed from the governing concept of natural gas or gasoline as LRF [26]. Bearing in mind prospective low- and zero-carbon alternatives, recent studies focus on exploring RCCI with methanol [27], ammonia [28] or hydrogen [29]. The last route is particularly attractive because hydrogen can be flexibly admixed at up to 25 % by volume with the natural gas supply chains, utilising the same on-board storage and injection infrastructure [30]. Although LRF choice can contribute to better RCCI performance, it should be considered primarily as a design criterion influenced by bulk fuel availability, rather than a technological improvement measure.

Within the topic of different fuel configurations for RCCI, there is scant research directed at the effect of HRF. This research direction seems particularly important from a feasibility perspective if drop-in alternatives to diesel are considered. Hanson et al. [31] tested DF and 20 % biodiesel blends as HRFs, while gasoline and gasoline-ethanol blends served as LRFs. In contrast to conventional diesel combustion (CDC), biodiesel blends in RCCI reduced HC and NO_X while increasing CO emissions. The counter-intuitive emission patterns were attributed to higher HRF concentration regions with lower local temperatures. Garcia et al. [32] performed comparative research, using gasoline as LRF, paired with one of three HRFs: DF, polyoxymethylene dimethyl ethers (PODE) and Fisher-Tropsh synthetic diesel with paraffinic makeup similar to hydrotreated vegetable oil (HVO). Notably, both synthetic diesels had high cetane numbers (CN) of above 70, thus providing a higher reactivity gradient than with DF. Results showed that the high CN of synthetic fuels advanced ignition at low load, while not affecting combustion duration. The HRF's effect diminished with an increase in engine load, which was attributed to increased LRF share in the mixture. Duraisamy et al. [33] performed comparative research on DF and PODE as HRFs, paired with methanol as LRF. Although the authors applied late HRF injection, they pointed out HRF's substantial effect on ignition. To achieve the same CA50 as for DF, the single start of injection (SOI) of PODE had to be delayed by 5 crank angle degree (CAD).

Considering NG as the primary fuel, Pinto et al. [34] used HVO and farnesane (bio-jet fuel) as HRFs in a single-cylinder engine. At 56 % NG/HVO blend ratio and late injection timings, typical for conventional dual-fuel combustion, the work demonstrated 83 % reduction in PM emissions, followed by corresponding reduction of 18 % in NO_X, compared to CDC. Significant penalty on HC and CO emissions was recorded. In a more recent study, Rimkus et al. [35] observed similarly insignificant effect of HRF on PM/NO_X trade-off. According to the authors, HVO contributed to a reduction in CO and HC emissions with respect to DF-activated conventional dual-fuel combustion. These studies, although important and comprehensive in terms of comparative fuel-to-fuel effects, do not provide conclusions that are directly relevant to ultra-lean RCCI combustion.

Sun et al. [36] compared DF and coal-to-liquid (CTL) fuel as HRFs, while gasoline served as LRF. Note that CTL had CN of 75 and paraffinic makeup similar to HVO. At single pilot injection, regardless of the SOI, switching to CTL advanced CA50 by 2–3 CAD, demonstrating the impact of CN on combustion timing. While advancing the SOI in certain mixture conditions, a rapid infliction point in CA50 monotony occurred, which the authors identified as mode-switching, between conventional dual-fuel and RCCI. Under RCCI regime, emissions showed simultaneous reduction in HC, CO and PM, by 22 %, 14 % and 60 % respectively, when DF was replaced by CTL fuel and the engine was recalibrated. NO_X emissions, however, were slightly increased.

A recent review by Gowthama Krishnan et al. [37] summarised the current progress in biofuel RCCI research. In terms of bio-LRF's, the oxygenated nature of alcohols was identified as a factor that improves combustion efficiency, allowing higher BR than gasoline. Regarding bio-HRF's, the study highlighted that fuel-bound oxygen can enhance NO_X formation while also improving combustion efficiency. In general, the authors postulated that further research should be angled towards extending the low-emission limits through dedicated calibration.

HVO has potential to change the paradigm of natural-gas diesel RCCI. It is a third-generation renewable fuel which can be flexibly produced from a variety of biomass feedstock [38,39], contributing to a more favourable GHG footprint on a well-to-wheel basis [40]. Its availability is currently scaled sufficiently for instant accommodation as diesel drop-in fuel (EN590 compatible) but its properties, largely better than diesel's, are not properly valorised in conventional diesel or conventional dual-fuel combustion. Hunicz et al. [41,42] postulated that HVO's very high CN enables superior single-fuel calibration when moving the paradigm to low-temperature, partially-premixed combustion with early sequential injections. Additionally, lower viscosity and higher volatility support better atomisation in an early injection regime, allowing more premixed mixtures without encountering wall-wetting.

Baškovič et al. [43] used HVO and methane-rich NG as the high- and low-reactivity fuels respectively for studying RCCI combustion. The EGR rate and energy share were used to optimise combustion and engine operation. A sensitivity analysis of the results showed that it is possible to achieve simultaneously ultra-low, engine-out emissions of NO_X, PM and particulate number (PN). The EGR rate should be kept below 30 % to avoid a significant increase in CO and hydrocarbons (HC) emissions. The study offered a complete engine calibration map for dual-fuel operation with HVO and natural gas. It proved that an engine with these two fuels can achieve ultra-low emissions while meeting the constraints of PRR and combustion stability. The study's main shortcoming is its applied focus, leaving a gap concerning the comparative analysis of the differences between HVO and conventional diesel in RCCI combustion.

Summarising the above discussion, it is well proven that HVO provides diesel-like performance in conventional CI engines, with minor benefits to emissions coming from its cleaner chemical make-up. The limited studies imply that HVO offers much wider calibration potential when used as a high-reactivity enhancer in dual-fuel engines operating in a low-temperature RCCI regime with natural gas. However, this potential is not explicitly characterised and the underlying factors are not well understood. Previous studies failed to provide a rigorous benchmark for HVO-NG in controlled RCCI conditions, by comparing it with DF-NG RCCI, and considered against the limits of CDC. In light of the referenced literature, the above knowledge gap currently meets the urgent need from the perspective of application. Next generation marine natural-gas engines realising RCCI combustion are approaching market implementation [23], justifying research investments into this technology.

This current work provides a comprehensive verification of the calibration potential of natural gas-based RCCI with HVO as high-reactivity fuel. The hypothesis is that high CN and greater volatility of HVO enable larger in-cylinder reactivity gradients at DF-like density stratifications. Building on these features, HVO-activated NG RCCI should allow significantly better NO_X/CH_4 trade-offs compared to its DF counterpart.

The verification experiments were performed on a state-of-the-art, single- cylinder research engine, with fully controllable/conditioned airpath and individual fuel path parameters, calibrated to relevant

emission levels in a CDC baseline. The RCCI calibration map covers the cross-sensitivity of HVO and DF to boost pressure, excess air ratio (λ), EGR rate and SOI. LRF/HRF blending ratios spanning from 83 % to 89 %, were used to support proper ignition onset while incorporating fuels of different reactivity. The magnitude of the results is condensed in the result section to the most relevant trends. An extensive network of sensors provided detailed combustion and emission characterisations, enabling relevant observations regarding the phenomenology of RCCI with different HRFs. The tailored approach allows the effect of individual HVO properties on particular aspects of the calibration to be decoupled.

2. Methods

2.1. Fuel specifications

Both HRFs used in this study, DF and HVO, were pump-grade fuels, subjected to detailed chemical and physical analysis to support the interpretation of the combustion and emission results. DF was a European commercial diesel, produced by Polish oil company Orlen. HVO was MY Renewable Diesel, produced by Finnish oil company Neste Oyj. Table 1 lists the fuels' key specifications, together with the relevant parameters of EN 590 and EN 15940, for DF and HVO respectively.

Table 1 shows that the key properties influencing spray atomisation – density and kinematic viscosity – have lower values for HVO than for DF. Lower density translates into lower droplet mass for the same volume. This leads to less momentum for fuel droplets ejected from the injector, which in turn results in poorer penetration and spray distribution. Lower viscosity improves the atomisation quality by reducing the energy requirement. It reduces the internal friction, meaning less energy is needed to atomise the liquid. This can lead to more efficient atomisation, where the energy is more effectively used to create a fine spray rather than overcoming the liquid's resistance. This positive effect on fuel atomisation and mixture formation was confirmed by numerical analysis provided by Cheng et al. [44] and empirical research by Hulkkonen et al. [45]. HVO exhibits shorter physical ignition delay than DF as a result of better fuel atomisation.

A higher CN denotes a shorter ignition delay, meaning that the fuel ignites more readily upon injection into the combustion chamber. This characteristic leads to more complete and efficient combustion, especially when the fuel is well-atomised into fine droplets. It is partially the result of abovementioned higher volatility, but stems mostly from HVO's paraffinic chemical make-up. For the same reason, HVO's hydrogen to carbon (H/C) ratio is higher than DF's, and thus has a higher LHV on a mass basis.

Both fuels meet the requirements of EN590′s sulphur limit. HVO's sulphur concentrations were below the equipment's accuracy threshold, indicating there was virtually no sulphur. This is expected, reflecting the feedstock used and the fact that hydrotreating further removes sulphur during production [46]. Note that sulphur in DF will promote the formation of particulate matter, regardless of the combustion regime [47].

The fatty acid methyl esters (FAME) content is derived from the compulsory biocomponent addition to commercial DF. The measured value (6.3 %) corresponds to the fuel categorisation stated by the manufacturer (B7 diesel). As a biofuel produced through hydro liquification, HVO does not contain any FAME. Furthermore, HVO's paraffinic structure means it contains hardly any aromatics, unlike DF. This reduces cancerogenic polyaromatic emissions and inhibits aldehyde formation [48].

To sum up, both the tested DF and HVO meet their respective standards for CI engine fuels. It is worth noting that the EN 15940 standard for HVO is more restrictive in several parameters than diesel's EN 590 standard.

Linde supplied the technical grade methane 2.5 (CH_4 concentration $\geq$ 99.5 %) used as low- reactivity fuel. As this is nearly pure CH_4, its physical and chemical parameters were not determined. A lower heating value (LHV) of 50 MJ/kg was used for estimation of engine thermal efficiency. This fuel is termed NG throughout the paper.

Table 1
Fuel specifications.

Parameter	Unit	EN 590	DF	EN 15,940	HVO
Density @ 15 °C	g/cm3	815 – 845	**828**	770 – 790	**778**
Kinematic viscosity @ 40 °C	mm^2/s	2 – 4.5	**2.94**	2 – 4	**2.86**
Lubricity @ 60 °C	µm	≤ 460	**406**	≤ 400	**344**
Cetane number (CN)	–	≥ 51	**55.3**	≥ 70	**90.7**
Flash point	°C	> 55	**66.3**	> 70	**68.2**
Lower heating value (LHV)	MJ/kg	NA	**43.6**	NA	**44**
Carbon	%wt.	NA	**86.6**	NA	**84.5**
Hydrogen	%wt.	NA	**13.1**	NA	**15.2**
Sulphur	mg/kg	≤ 10	**6.1**	≤ 5	**< 1**
Water	mg/kg	200	**38**	200	**17**
Fatty acid methyl ester	%V/V	≤ 10	**6.3**	0	**0**
Aromatic hydrocarbon	%V/V	NA	**26.8**	NA	**< 1**
Distillation					
10 %vol.	°C		**213**		**258**
50 %vol.	°C		**274**		**278**
90 %vol.	°C		**334**		**290**
95 %vol.	°C		**351**		**294**

2.2. Experimental setup

A state-of-the-art, single-cylinder AVL 5402 research engine was used to assess the effects of different HRFs on RCCI combustion and emission. Table 2 lists the engine's governing parameters. Fig. 1 is a test stand schematic diagram, with emphasis on its air and fuel paths. The combustion system consisted of a four-valve head and a toroidal in-piston combustion chamber.

The liquid fuel conditioning system consisted of an AVL 753C temperature controller and an AVL 733S dynamic fuel meter. A Bosch CP 4.1 high-pressure pump supplied fuel into the combustion chamber through an eight-hole electromagnetic injector with a 151° spray angle. The interactions between the developing spray and combustion chamber at characteristic CADs are schematically depicted in Fig. 2. The ETAS INCA software and the fully open Bosch controller were used to govern injection parameters.

From Fig. 2, one can note, that for gross of RCCI conditions explored in this study, where injection ends earlier than 35 CAD before top dead centre (bTDC), all the fuel is injected to the squish region. As the liquid fuel values in RCCI are low, the spray is completely evaporated before it

Table 2
Research engine data.

Type	AVL 5402
Configuration	four-stroke, single-cylinder
Bore	85 mm
Stroke	90 mm
Connecting rod length	138 mm
Displacement	510.5 cm^3
Compression ratio	17:1
No. of valves	4
Swirl ratio	1.7
Combustion type	direct injection
Injection system	common rail, Bosch CP4.1
Fuel injector	electromagnetic, 8-hole x 0.12 mm, 151° incl. angle
Max. fuel injection pressure	180 MPa
NG fueling system	mass flow controler, M + W Instruments D-6300
Boost system	electrically driven Eaton M45 compressor
EGR system	high pressure, cooled
Engine management	AVL-RPEMS, ETK7-Bosch
In take valve opening	712 CAD
Intake valve closing	226 CAD
Exhaust valve opening	488 CAD
Exhaust valve closing	18 CAD
Max. engine IMEP	2.4 MPa

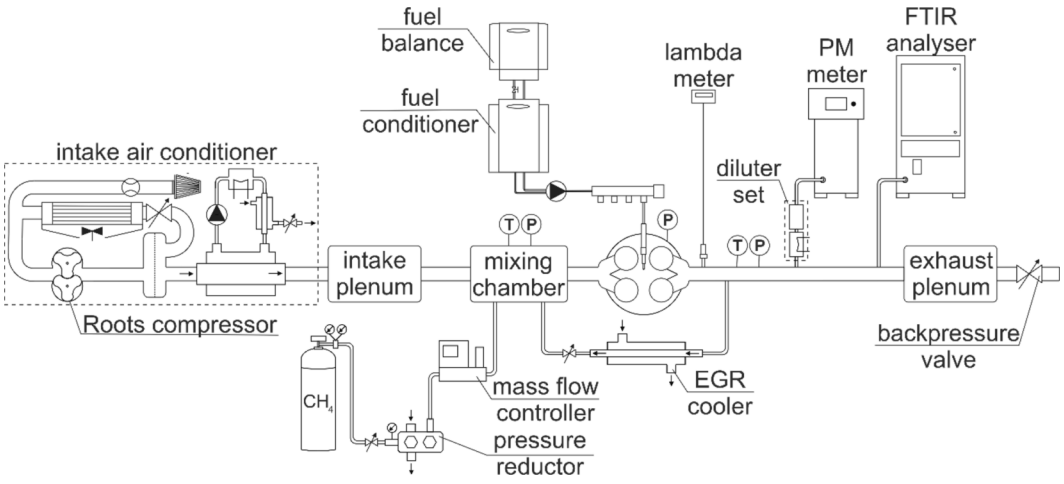

Fig. 1. Diagram of the engine air and fuel paths.

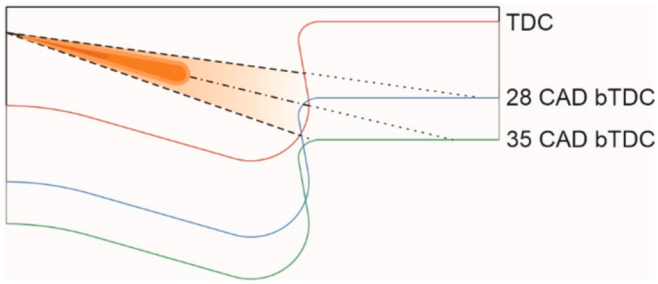

Fig. 2. Spray-combustion chamber interactions at the characteristic crank angle positions. At 28 CAD the spray is equally distributed between the combustion bowl and squish region.

reaches the liner. The upward movement of the piston creates a tumble motion that supports re-distribution of high-reactivity fuel towards the cylinder centerline. Hence, at start of combustion, the in-cylinder mixture will have the highest reactivity near the cylinder liner, and monotonically decreasing towards the centerline. Note, that the design of experiment elaborated in this study, also explored boundary conditions of RCCI combustion. I.e. the injection timings that target re-distribution of high reactivity fuel between squish region and combustion bowl. When analysing these results, one should mind more complex reactivity patterns.

Gaseous fuel was stored in a 200-bar cylinder and port fuel injected after the pressure reduction to 280 kPa by a heated pressure regulator. Gas was admitted with constant flow using a mass flow controller (M + W Instruments Mass-Stream D-6300) calibrated to CH_4. The gaseous fuel and recirculated exhaust gas were mixed with intake air in a plenum chamber to homogenise the mixture before entering the cylinder. An Eaton M45 Roots compressor powered by an 11-kW electric motor provided boost pressure. The air downstream of the compressor was thermally stabilised with the use of gas exchangers and a mixing valve. The exhaust system was equipped with a backpressure valve. This mimicked turbocharger operation, enabling high-pressure EGR and preventing NG scavenging during the valve overlap. A thermal conditioning system was used to maintain coolant and lubricant temperatures with +/- 0.5 °C accuracy. A Bosch LSU 4.2 lambda probe and ETAS LA4 lambda meter were used to measure the excess air ratio, with consideration of pressure compensation.

Combustion was analysed from a high-speed pressure signal coming from an AVL GU22C piezoelectric pressure transducer, triggered by an optical encoder, with a constant angular resolution of 0.1 CAD. The concentrations of 20 regulated and unregulated exhaust gas components were determined using AVL's Fourier transform infrared (FTIR) multi-component analytical system. Particulate size distribution was determined with TSI's EEPS 3090 particle size spectrometer, employing the electrical mobility measurement principle. The particle size measurement ranged from 5.6 to 560 nm, within 32 size channels. Table 3 presents the main parameters of the measuring equipment.

All slow-changing parameters, such as air and fuel flow rates, temperatures, excess air ratio (λ) and average intake/exhaust pressures, were recorded using an in-house measurement system and time-averaged. Exhaust concentrations and particle size distributions were recorded simultaneously with the other parameters and then averaged.

2.3. Design of experiments

2.3.1. Reference conditions for CDC and RCCI experiments

A detailed examination was conducted at a single engine-speed and

Table 3
Engine test bench measurement equipment and accuracy.

Measurand	Transducer	Meas. range	Accuracy
In-cylinder pressure	AVL GU22C	0–25 MPa	0.25–1.0 %[1)]
IMEP stability		N/A	3 %
Liquid fuel consumption	AVL Fuel Mass Flow Meter 733S	0–125 kg/h	0.12 %
Gaseous fuel consumption	M + W Instruments D-6300	0–120 Nl/min	2 %
Excess air ratio (λ)	Bosch LSU 4.2 / ETAS LA4	0.7–2.8	1.5 %
Air mass flow rate	E + E Elektronik EE741	2.6–1000 kg/h	3 %
Intake/exhaust press.	WIKA A-10	0–4 bar	0.5 %
Temperatures (ambient, intake air, EGR, cooling, oil, fuel)	Pt100 Czaki TP-361	−40–400 °C	0.2 %
Exhaust temperature	Thermocouple K Czaki TP-204	0–1200 °C	0.8 %
Exhaust composition (gaseous compounds)	AVL Sesam FTIR CO:	1–10000 ppm	0.36 %
	HC:	1–1000 ppm[2)]	0.1–0.49 %[3)]
	NO_X:	1–4000 ppm	0.31 %
PM/PN	TSI EEPS 3090	5.6–560 nm[4)]	N/A

[1)] Depending on temperature.
[2)] Given measurement span relates to the concentration of a single identified hydrocarbon
[3)] Depending on the type of hydrocarbon species.
[4)] Particle size range.

load setpoint. This was the basis to compare combustion evolution, efficiency and emissions parameters for CDC and RCCI with two high-reactivity fuels. Engine speed was controlled at 1500 rpm. At the same time, the total fuel value (the sum of injected fuels masses multiplied by their LHVs) was kept the same for all fuel and combustion mode combinations. This resulted in a slight load variation around the CDC DF reference of 0.8 MPa indicated mean effective pressure (IMEP), dictated by changes in indicated efficiency.

Note that the engine control parameters in CDC were tuned to achieve low emissions while maintaining high thermal efficiency. This was accomplished with split injection (pilot fuel and main fuel) with respective SOIs denoted as SOI_1 and SOI_2 (see Table 4).

The reference operating conditions for RCCI mode with DF were selected to provide stable operation with a reasonable trade-off between NO_X and CH_4 emissions. The performance target was to obtain similar CA50 which secured high efficiency for CDC combustion mode, with the corresponding manifold absolute pressure (MAP) and temperature (fixed at 26 °C in both cases). Only BR and the diesel SOI were regulated. The targets were achieved with a single injection of high-reactivity fuel, applied at SOI of 40 CAD bTDC. This provided distinctive separation between injection and ignition events, ensuring that the ignition delay depended solely on the fuel's chemical reactivity. Injection pressure was set at the same 800 bar reference in both CDC and RCCI.

All engine control parameters remained unchanged when replacing DF with HVO, thus highlighting the effect of high-reactivity fuel in RCCI. Table 4 gives details about the critical airpath and fuelling setpoints for the reference CDC and RCCI cases.

2.3.2. Sensitivity to RCCI control parameters with DF and HVO as high-reactivity fuels

After the initial characterisation of fuel-to-fuel differences at reference conditions, the experiments with HVO and DF focused on exploring the fuel responses to the most significant RCCI control parameters. To this end, three independent sweeps were designed around the reference RCCI setpoints, depicted in Table 5.

Boost pressure sweep was performed for a single high-reactivity fuel injection at SOI 40 CAD bTDC. The fuel pressure was set to 800 bar. NG energy fraction, denoted as BR was approximately 85 % (fuel mixtures denoted as DF-NG-85 and HVO-NG-85). Additional tests with BR increased to 89 % (HVO-NG-89) also were performed. MAP was varied from atmospheric to 190 kPa or to the misfire limit, whichever came first. Independently of boost pressure, the intake air temperature was constant at 26 +/-1 °C. The exhaust backpressure was maintained 2–4 kPa higher than MAP for all experiments, mimicking turbocharger operation.

SOI sweep was performed at a constant MAP of 140 kPa +/- 2 kPa. The thermal conditions and fuel mixtures were the same as for the boost sweep. The earliest SOIs were determined by misfire limits, whereas the sweep progressed until NO_X or PM limits of the analysers were exceeded.

EGR sweep was performed for DF-NG-85 and HVO-NG-85 fuelling strategies, 140 kPa boost pressure and 40 CAD bTDC SOI. The air/exhaust mixture temperature was left uncontrolled: it varied between 26 and 50 °C, depending on the EGR rate.

The above-mentioned parameters were further explored in combinations with each other and while changing the energy-based BR from 83 % to 89 %. The complete experimental matrix summarised in Table 5 was dictated by the results of the initial parameter sweeps, performed to comprehensively understand the effect of different high-reactivity fuel on RCCI combustion. The selection of these combined sweeps is designed to support the reader's comprehension of the governing responses.

Table 4
Reference setpoints for CDC and RCCI for different tested fuels.

Parameter/mode	CDC	CDC	RCCI	RCCI
Fuel	DF	HVO	DF-NG-85	HVO-NG-85
BR by energy	0	0	83.8 %	83.2 %
SOI_1 [CAD bTDC]	15	15	40	40
SOI_1 mass fraction	7 %	7 %	100 %	100 %
SOI_2 [CAD bTDC]	5	5	–	–
MAP [kPa]	138.6	139.8	139.6	140.6
λ	2.35	2.38	2.33	2.21
IMEP [MPa]	0.807	0.804	0.827	0.772

Note that all experiments were performed at stable engine coolant and oil temperatures, both set to 85 °C. The intake air temperature was also fixed, at at 26 +/-1 °C, to provide a straightforward comparison for both combustion modes.

Table 5
Detailed engine control parameters for performed parameter sweeps.

Control variable	HRF	BR [%]	HRF SOI [CAD bTDC]	MAP [kPa]	Intake temp. [°C]	EGR [%]	λ[-]
MAP	DF	85	40	101…190	26	0	1.87…2.72
MAP	HVO	84	40	100…188	27	0	1.82…2.76
MAP	HVO	89	40	100…178	27	0	1.84…2.66
SOI	DF	84	45…25	139	26	0	2.34
SOI	HVO	85	60…35	140	27	0	2.25
SOI	HVO	89	50…25	140	27	0	2.29
EGR	DF	83	40	140	26…47	0…22	2.28…1.69
EGR	HVO	83	40	140	27…49	0…22	2.19…1.64

2.4. Post-processing methods

The in-cylinder pressure signal was recorded with a 0.1CA resolution, for 100 consecutive cycles at each operating point. This provides an accurate estimation of IMEP and HRR-based values [49,50]. The repeatability of the combustion process was automatically monitored, with the co-variance (CoV) of IMEP < 4 % as stability criterium. The raw, relative in-cylinder pressure was pegged, using the intake and exhaust pressure as reference, and then filtered.

The combustion analysis was performed on cycle-averaged signals, and encapsulated the calculation of IMEP, PRR, heat release rate (HRR) and bulk in-cylinder temperature. IMEP and PRR are standard in engine research and for their calculation method one can refer to Heywood [51]. Net IMEP was further used to calculate ITE, using the LHV-weighted individual fuel consumptions (LRF and HRF) as inputs. Note, that in laboratory-type single-cylinder engine research, relying on indicated-specific approach to calculate power-related values is considered more reliable than brake-specific nomenclature typically used for multi-cylinder engines [52]. Consequently, all postprocessed values based on power definition, used in this study are considered as indicated-specific.

The statistical error in ITE was assessed using the total differentiation method, where the measurement uncertainties in fuel consumptions (DF and NG) were determined based on the standard deviation from multiple measurements. Additionally, the error in determining IMEP was provided by the pressure sensor manufacturer. In all cases, the maximum ITE error was between 4 % and 5 % with the highest contribution of IMEP determination uncertainty (Table 3).

The HRR is calculated using the first law analysis with an instantaneous ratio of specific heats dependent on mixture temperature and composition. To satisfy this, the external EGR rate was calculated by comparison of air flow with and without EGR, with consideration of the intake fluid density, resulting from intake temperature. Following the above port-flow composition estimation, an isentropic gas-flow model produced the total trapped mass (aspirated and residuals), based on the port and in-cylinder thermodynamic conditions. The instantaneous bulk

temperature was further calculated from the in-cylinder pressure, using the equation of state, with HRR dictating the changing mixture composition.

The HRR values in the paper are net, and consider the heat transfer through the cylinder walls, estimated by the Hohenberg correlation [53]. Cumulative net heat release (CHR) was further used to determine the crank angles of 5 % and 50 % mass burned (CA05 and CA50, respectively), used as combustion onset quantifiers in this study.

The molar concentrations of exhaust gas components, measured directly using "wet" effluent gases, were converted to indicated specific emissions, considering atomic fuel composition, excess air ratio and specific fuel consumption. The PM concentrations were calculated based on the size distribution, with the assumption of 1 g/cm^3 particle density. The mass per volume concentrations were then converted to indicated-specific emission values.

3. Results and discussion

3.1. Benchmarking DF and HVO at reference CDC and RCCI combustion modes

3.1.1. Performance of HVO and DF in CDC mode

Fig. 3a shows that switching the fuel from DF to HVO has negligible effects on the in-cylinder pressure trace in CDC mode. This is in line with the well-established view of HVO as a renewable drop-in alternative for diesel. HRR plots in Fig. 3b give a deeper insight into the combustion characteristics. In CDC (dashed-lines), HVO's significantly different reactivity has a very small effect on the course of combustion during the first premixed phase. This is because the ignition of the pilot is mainly controlled by spray evaporation and oxidiser entrainment. HVO's pilot ignition is only around 1.5 CAD earlier, mainly attributed to improved spray atomisation, fostered by the fuel's lower density and kinematic viscosity. Notably the slight differences in the pilot combustion between HVO and DF are furthered hindered during the diffusion-controlled combustion phase, which commences almost instantly after the main injection (initiated at 5 CAD bTDC for both fuels) reaches the burning zone of the pilot. Careful analysis shows that HVO main combustion initiates around 0.7 CAD later than with DF, as the earlier-initiated pilot zone combustion is almost concluded before the main injection commences. This means that the chemical activity from the pilot is largely quenched before the main injection commences and proves that fuel (as soon as it is above the threshold set by the EN590 standard) does not significantly affect CDC combustion.

The above details concur with the current state of the art in combustion phenomenology of HVO [54,55]. The main takeaway is that, from the engine performance perspective, DF and HVO have nearly identical combustion characteristics in CDC mode, despite significantly different.

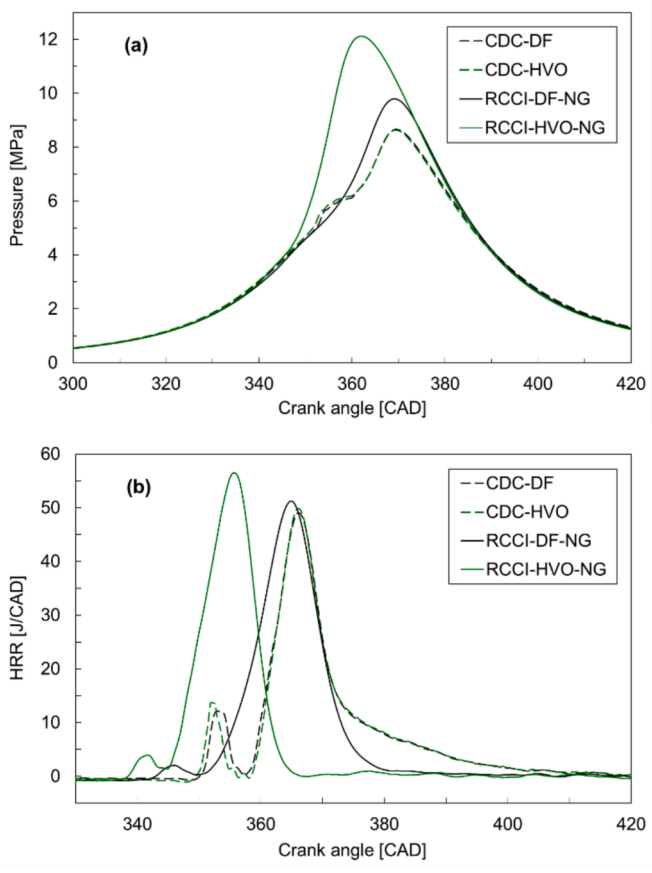

Fig. 3. Comparison of pressure (a) and HRR (b) for CDC and RCCI combustion under the reference conditions, specified in Table 4.

3.1.2. Reference RCCI operation with DF and NG

The results obtained for CDC and their agreement with the state of the art in HVO research, give credibility to the new results obtained for RCCI mode. Contrary to CDC, and accordingly to the premise of the present study, HVO exhibits large-scale differences in the LTC regime where the heat release is controlled by fuel reactivity. This is immediately evident in Fig. 3a, where HVO (green solid line) supports noticeably earlier and more rapid combustion, resulting in high peak in-cylinder pressure.

Fig. 3b shows RCCI HRR profiles have phenomenologically similar form for both DF and HVO. The HRR starts with a small peak caused by the pre-ignition and negative temperature coefficient reactions. These reactions usually start locally, in the regions of the cylinder where the high-reactivity fuel density is the highest, i.e., around the cylinder liner [16]. They do not produce much heat but generate hydroxyl (OH) radicals that trigger an almost-volumetric in nature, but reactivity stratification-controlled, main combustion event. This commences at around 350 CAD for DF. Note that the ignition delay is around 30 CAD with the given combustion chamber design, so the main LTC phase is fully premixed and completely decoupled from the spray development.

Benchmarking the DF-RCCI reference against the CDC point with the same boost pressure, (Table 6), highlights RCCI's potential to achieve significantly higher ITE. RCCI's net efficiency peaks around 45 %. This is predominantly attributed to shorter (half that of CDC), yet still correctly phased, combustion. The onset of the peak heat release close to TDC (CA50 at 364 CAD for RCCI reference) transfers the pressure rise rate most effectively to useful work, while minimising cylinder heat losses. At the same time, lack of local fuel-rich regions allows RCCI to reduce

Table 6
Performance and emission results for HVO and DF, at reference CDC and RCCI combustion modes respectively.

Parameter/mode	CDC	CDC	RCCI	RCCI
Fuel	DF	HVO	DF-NG-85	HVO-NG-85
CA05 [CAD]	353.7	353.4	355.4	348.8
CA50 [CAD]	367.9	367.7	364.8	354.9
CoV-IMEP-[%]	0.76 %	0.82 %	3 %	2.92 %
ITE [%]	42.7 %	43.2 %	44.8 %	41.6 %
Indicated specific emissions:				
CO_2 [g/kWh]	602	589	463	499
CO [g/kWh]	0.46	0.33	2.91	2.23
CH_4 [g/kWh]	0.0004	0	9.93	5.37
NMHC [g/kWh]	0.38	0.29	0.95	0.79
NO_X [g/kWh]	6.25	6.36	2.25	7.04
PM [mg/kWh]	72	41.9	1.14	4.59
PN [cm^{-3}]	21×10^6	17.1×10^6	1.59×10^6	1.52×10^6

the peak combustion temperature, resulting in 64 % lower NO_X output. The PM is cut close to the levels that are almost untraceable from the perspective of measurement device accuracy. CO and HC, particularly methane slip, remain excessively problematic for NG-based RCCI. Note however, that the reference RCCI point is realised with a diesel-stock combustion chamber, without exploring any airpath-related co-optimisation measures (same boost pressure and intake temperature as DF). For example, reducing the upper crevice volume by piston crown chamfering, or other hardware measures explored in dedicated gas engines, can reduce methane slip by as much as 70 % [56].

3.1.3. RCCI reference with HVO as high-reactivity fuel

Table 6 shows that realising the DF – RCCI reference setpoint with HVO as high-reactivity fuel causes a deterioration in the thermal efficiency, because combustion happens far too early with the given air/fuel control setpoints. At the same time, excessive peak pressure and hence, elevated bulk compression temperature, pushes the NO_X emissions back up to diesel-like levels, yet with significantly reduced methane slip. A shorter mixing time also increases PM mass emission for HVO, though it is still an order of magnitude lower than for CDC. Notably, RCCI creates finer particles than CDC, regardless of the fuel used, as shown in Fig. 4. Comparing PM size distribution for DF and HVO in RCCI mode, unlike CDC, DF produces more fine particles, which can be attributed to longer mixing time. On the other hand, HVO produces more PM in accumulation mode, for the same reason.

3.2. RCCI calibration potential with HVO

The results presented in previous section prove the first part of this paper's initial thesis regarding the effects of HVO reactivity. While providing diesel-like performance in CDC, HVO has a profound impact when used as a pilot fuel for low-temperature RCCI combustion. The HVO results discussed in section 3.1.3 show deteriorations in engine performance and NO_X emissions when compared with the DF-RCCI reference, but these are caused by premature ignition in the diesel-calibrated RCCI regime. Crucially, the results indicate a wide space for optimisation without hitting the misfire limits. The present section evaluates this potential by exploring the HVO response to typical RCCI control variables. The results are compared with the same parameter sweeps performed with DF. The aim is to provide a link with existing knowledge on RCCI, and underline the differences while operating with fuel of much higher reactivity.

3.2.1. Sensitivity to fuelling parameters

RCCI can be controlled with two governing fuel control parameters. The BR between the high- and low-reactivity fuels usually provides the largest sensitivity, while the SOI of the high- reactivity fuel allows fine tuning of the balance between the combustion phasing and emissions. These results are presented for HVO and DF in Figs. 12-14. The SOI sweep was performed around the reference point of SOI of 40 CAD discussed in the previous section, which implied increasing the BR to mitigate the premature combustion for highly reactive HVO.

Fig. 5 shows that adjusting the BR to 89 % allows retention of diesel-like phasing while operating RCCI on highly reactive HVO. Decreasing the HVO rate in favour of NG by three percentage points delays combustion by around 10 CAD for the reference SOI. The SOI provides similar responses for both fuels, and for the same BR, reference CA50 of approximately 365 CAD can be achieved for HVO for baseline at 55 CAD bTDC. The trend is an order of magnitude lower than for BR, yet sufficiently significant to consider SOI as a control parameter.

Comparing Fig. 5 and Fig. 6 clearly shows that CA50 around 365–370 CAD provides the highest indicated efficiency, regardless of the high-reactivity fuel used. RCCI efficiency peaks at 44.2 % ITE, achieved for HVO-NG 85 at the mentioned SOI of 55 CAD and the given airpath settings. Injecting later provides a monotonic decline of ITE as the CA50 moves before TDC, resulting in negative work done on the piston by combustion.

Cycle-to-cycle variability increases as injection moves earlier. Fig. 7 shows that CoV in IMEP correlates directly to late combustion phasing, with fuel effect having a secondary order influence. The stability criterion of CoV in IMEP < 4 % is exceeded at the threshold CA50 of approximately 370 CAD, regardless of whether HVO or DF is used, and regardless of the ratio of these fuels to NG. Peak ITE in RCCI is thus tightly constrained by the combustion stability boundary conditions for early SOIs. For instance, for the BR of 89 %, injecting HVO only 5 CAD earlier than the optimum SOI of 55 CAD bTDC results in ITE deteriorating by as much as 6.5 percentage points. The same trend can be seen for other fuelling/BR choices when the SOI is advanced from their respective peak ITE setpoint.

Flame quenching is the direct cause of both the increased cycle-to-cycle variability and the cycle-averaged ITE collapse. Confirmation of this is found in the emission results, particularly the CH_4 and CO emissions presented in Fig. 8 and Fig. 9 respectively. The CH_4 emissions escalate beyond the scale of Fig. 8 for early SOI setpoints, correlating to the previously mentioned drop in efficiency. The same happens for CO, indicating that, during expansion, the combustion quenches before reaching the HVO/DF lean regions near the centreline of the cylinder. The increased cycle-to-cycle variability stems from the feedback mechanism associated with reactivity-controlled combustion concepts. This mechanism has been extensively studied by the authors in earlier works on HCCI [57] and RCCI [21]. Consecutive cycles with poor combustion efficiency transfer some of the combustion by-products to the next cycle as retained residuals. Consequently, the next cycle tends to ignite earlier due to the presence of highly reactive products of partial combustion

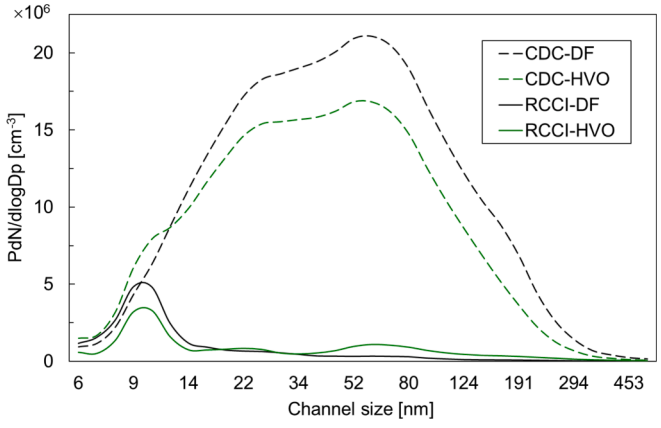

Fig. 4. Particulate size distributions for CDC and RCCI combustion under the reference conditions, specified in Table 4.

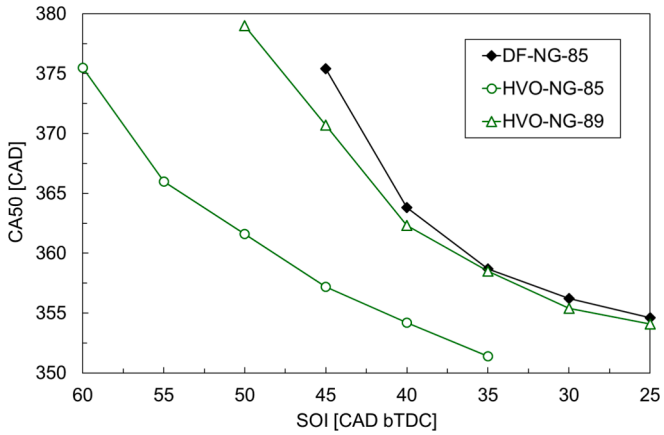

Fig. 5. CA50 for tested fuel configurations at variable SOI of HRF.

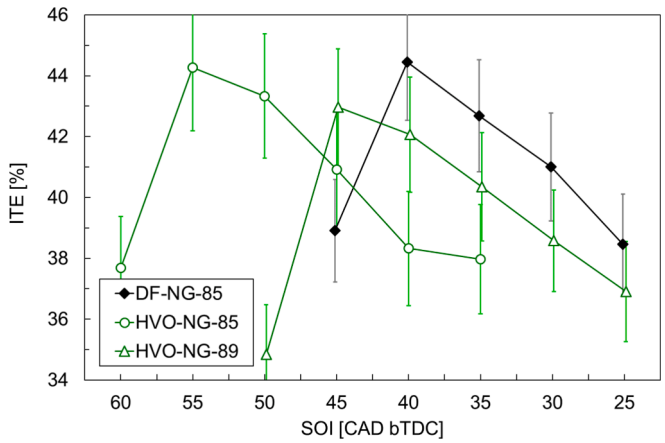

Fig. 6. ITE for tested fuel configurations at variable SOI of HRF. Error bars show maximum statistical uncertainty.

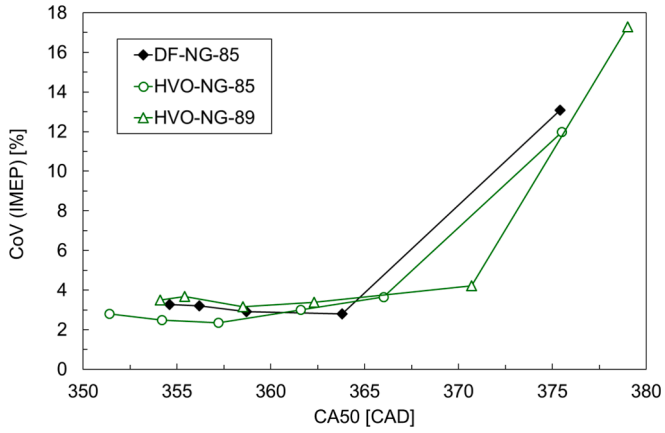

Fig. 7. The effect of CA50 on CoV in IMEP at variable SOI of HRF.

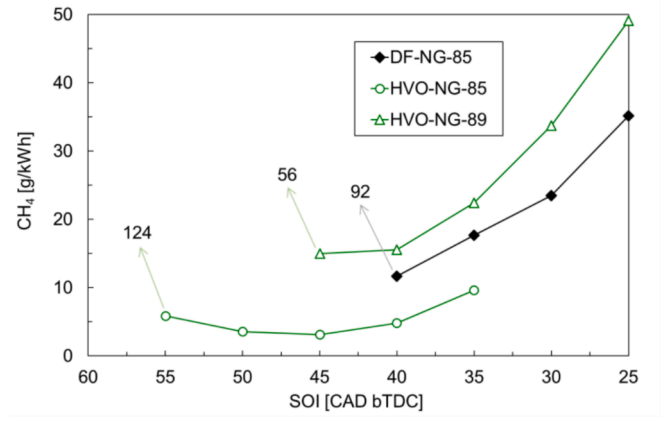

Fig. 8. Emissions of CH_4 for tested fuel configurations at variable SOI of HRF.

giving it a larger overall fuel value. Thus, the CoV in IMEP increases with the higher the unburned fraction, and in general, with the higher the amount of retained or recirculated residuals. This will become evident in the following sections, which study the effect of airpath parameters, including scavenging.

Focusing on absolute emission results, Figs. 8-9 clearly show that the highest overall fuel reactivity (i.e., HVO-NG-85 case) supports more complete combustion, which for optimised combustion phasing (SOI = 55 CAD bTDC) produces around 6 g/kWh and 4 g/kWh for CH_4 and CO respectively. These values are still very high, but nevertheless are promising, considering that HVO's high reactivity accommodates further mixture dilution, allowing later SOIs where the CH_4 emissions reaches their local minima. Airpath calibration measures are discussed in the following section, but at this point one can note that CH_4 emissions exhibit a distinctive minimum in the middle of the explored SOI range. This non-monotonic trend is evident for all fuel/BR cases in Fig. 8. It is typical for RCCI combustion because moving towards later SOIs gradually increases the share of flame propagation in the DF fuel mode, gradually departing from the pure RCCI concept. NG is more prone to quench around the local fuel-rich flame kernels at high air–fuel ratios than with volumetric combustion [21]. Moreover, the same trend exists for CO emissions, as shown in Fig. 9, but the minimum does not quite overlap with the lowest CH_4 emission points. However, the trade-off is not large, because the CO emissions, outside the quenching/misfire regime, are less sensitive to SOI.

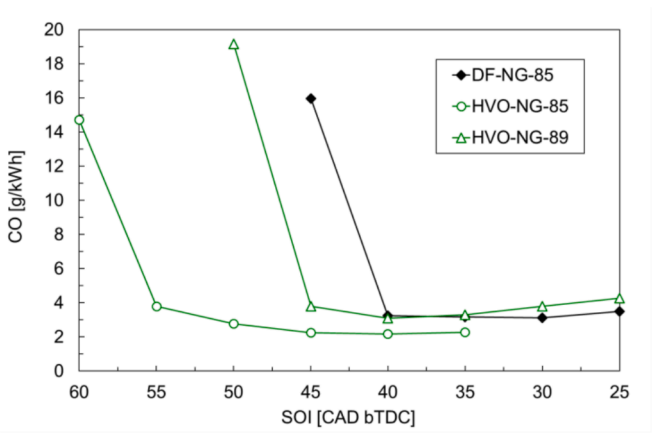

Fig. 9. Emissions of CO for tested fuel configurations at variable SOI of HRF.

Retarding the SOI from the peak ITE point not only increases CH_4 but as the mixture becomes less diluted, the elevated local temperatures have a negative effect on both NO_X (Fig. 10) and PM emissions (Fig. 11) which grow exponentially towards a conventional dual-fuel regime. NO_X can kept near 0.4 g/kWh at the RCCI points that exhibit maximum efficiency. That is low enough to meet the proposed forthcoming EPA Tier 5 non-road mobile machinery (NRMM) limit without aftertreatment [58].

The same SOI settings minimise CH_4 and PM emissions (Figs. 8 and 11). However, even when increased by later SOIs (less mixing time – more locally rich mixture), PM is not a particularly worrisome problem for dual-fuel combustion with natural gas because it is still an order of

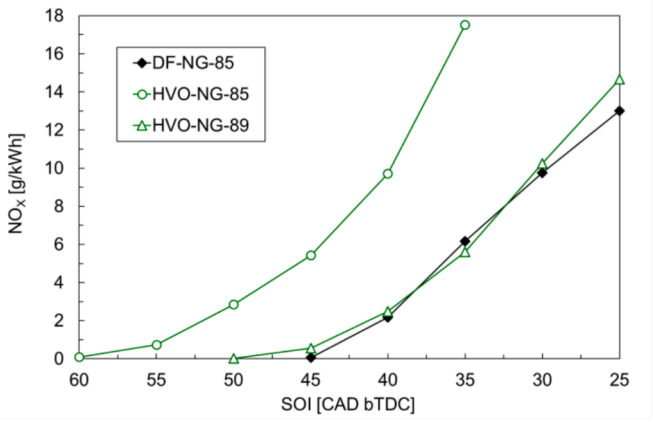

Fig. 10. Emissions of NO_X for tested fuel configurations at variable SOI of HRF.

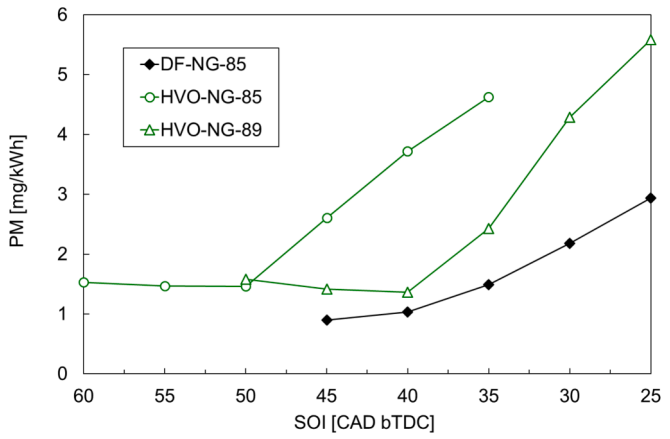

Fig. 11. Emissions of PM for tested fuel configurations at variable SOI of HRF.

magnitude lower than for CDC. The PM values of 1–5 mg/kWh recorded for RCCI, regardless of the fuel, are far below the current EPA Tier 4 NRMM limits, considered here as a benchmark. The trends in PN (not shown graphically) are unclear and non-monotonic. However, the quantities are small, from 1 to 2 $\times$ 10^6/cm^3. Based on the size distribution, advance of SOI from 40 to 55 CAD bTDC increases the concentration of particles in nucleation mode by 20 %, while reducing the number of particles in accumulation mode by 30 %, with nearly constant PN. Given the earlier remark on relevance and applied focus of this paper, PN and its distribution is not discussed further, as it deserves a dedicated, more fundamental-level study.

3.2.2. *Sensitivity to boost pressure and excess air*

Fuelling parameters can be varied using fast measures that also enable cycle-to-cycle control, but the airpath provides a slower response rate in real engines restricted by turbocharger inertia, for example. The results in this section cover RCCI response to boost pressure (MAP). This was varied around the reference value of 140 kPa, hence covering the λ range from approximately 1.9 to 2.3 (see Table 5 for details). Both MAP and λ are denoted on the horizontal axes of Figs. 12-18, on the lower and upper scales respectively. Note that the results for HVO cover two BR – the reference 85 % and the reduced reactivity blend of 89 %.

The effect of mixture strength on combustion phasing (Fig. 12) is mostly monotonic, except for the lack of sensitivity around the naturally aspirated conditions (MAP of 100 kPa). HVO results, statistically, have the same gradient as DF, with an offset dictated by the fuel reactivity. Note that, phenomenologically, the effect of elevating boost pressure is

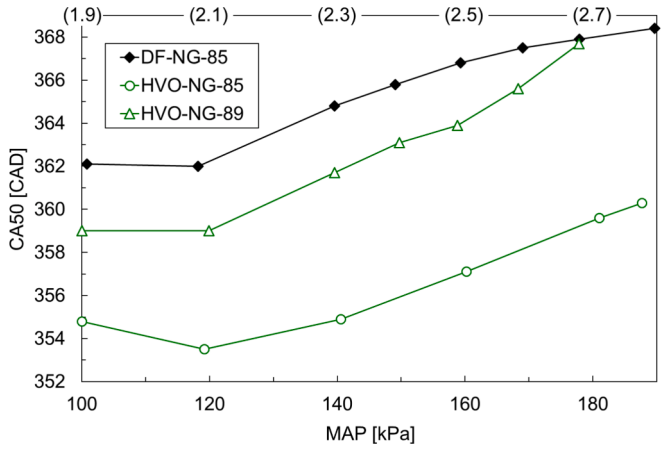

Fig. 12. CA50 for tested fuel configurations at variable MAP (approximate λ values are provided in brackets).

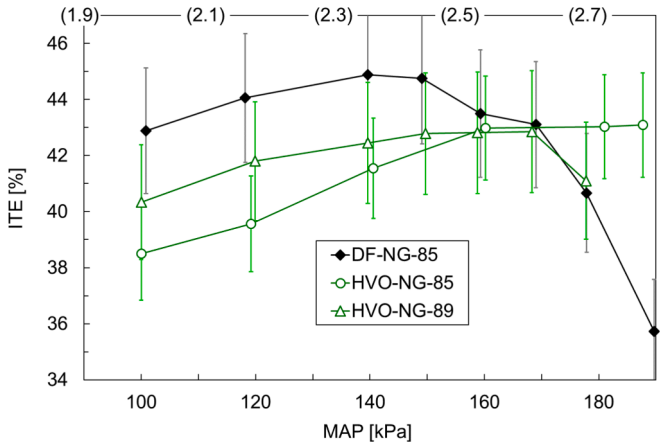

Fig. 13. ITE for tested fuel configurations at variable MAP (approximate λ values are provided in brackets). Error bars show maximum statistical uncertainty.

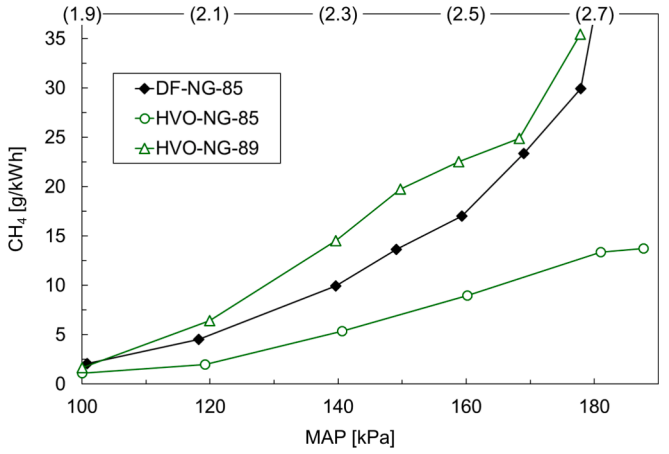

Fig. 14. Emissions of CH_4 for tested fuel configurations at variable MAP (approximate λ values are provided in brackets).

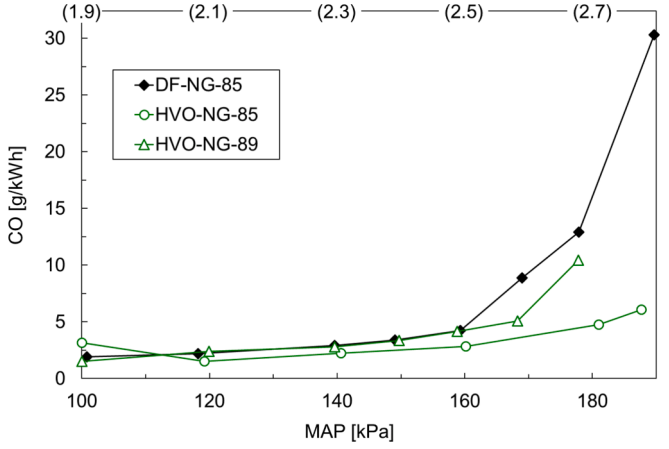

Fig. 15. Emission of CO for tested fuel configurations at variable MAP (approximate λ values are provided in brackets).

somewhat similar to advancing the injection timing, i.e., fuel dilution increases. However, SOI advancement does it locally, affecting only the HRF dilution, whereas increasing the boost pressures dilutes the total fuel mixture, including NG. These effects can be seen in the CA50 results,

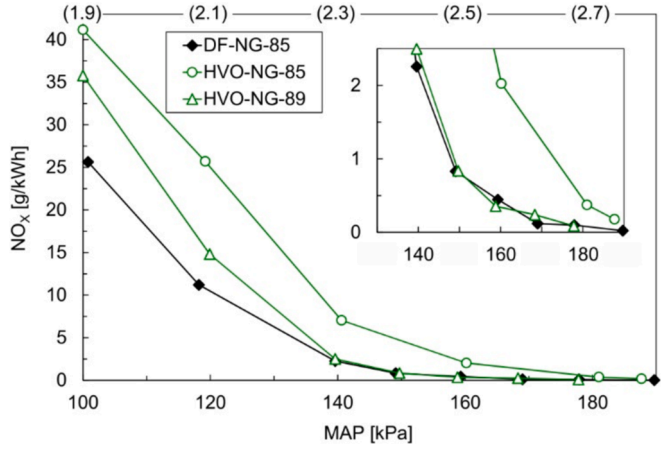

Fig. 16. Emissions of NO_X for tested fuel configurations at variable MAP (approximate λ values are provided in brackets).

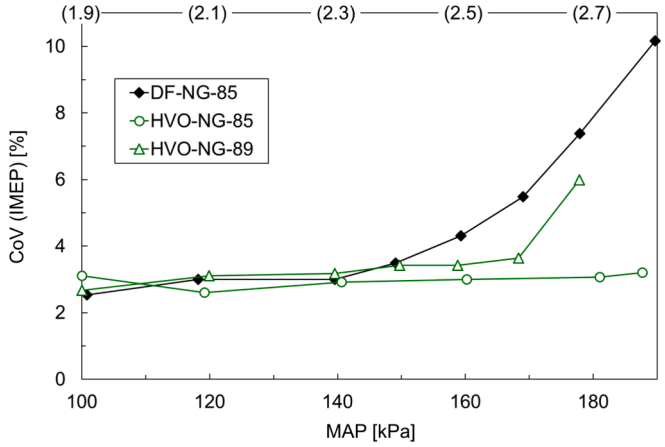

Fig. 17. CoV in IMEP for tested fuel configurations at variable MAP (approximate λ values are provided in brackets).

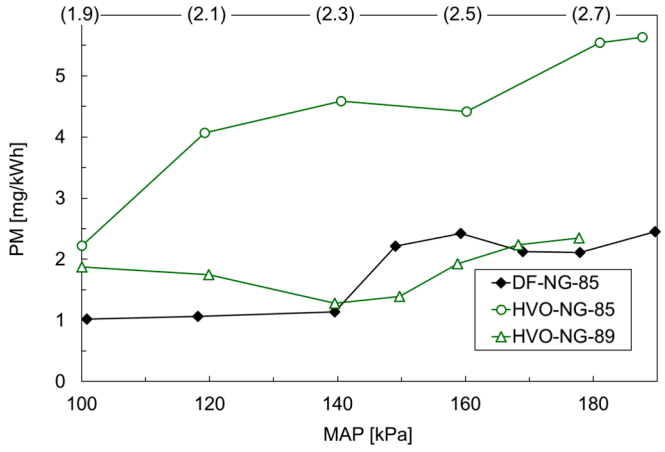

Fig. 18. PM emissions for tested fuel configurations at variable MAP (approximate λ values are provided in brackets).

as diluting the HRF causes later ignition, resulting in later combustion phasing. The fact that the LRF is also diluted slows down the reaction kinetics, further increasing the CA50 values.

The trends in ITE, shown in Fig. 13, are a superposition of CA50 figures, which determine the thermodynamic efficiency of the cycle, and combustion efficiency. Comparing Fig. 12 and Fig. 13, one can observe that ITE reaches the peak value where the combustion is optimally phased (around TDC). This is why HVO efficiency optimises at larger boost pressures than for DF. However, it does not yield as high ITE as is achievable with DF. This is because the mixture becomes too lean to support complete combustion of natural gas, particularly in the parts of the cylinder not sufficiently seeded with HVO. Consequently, methane slip increases at higher MAP values, as seen in Fig. 14.

Increased BR means the volumetric ratio of lean NG increases, explaining why the HVO-NG-89 case results in the steepest CH_4 emissions gradient. Note that CO emissions (Fig. 15) also increase with MAP. This is through the same phenomena, but the growth rate is partially compensated by the increased global air excess, supporting oxidation of CO to CO_2 when combustion quenches. On the other hand, realising RCCI with reference HVO-NG BR of 85 % tends to be the most resistant to mixture dilution, and hence produces the smallest cumulative hydrocarbon emissions at high λ values. This is another indication that HVO offers wider RCCI calibration opportunities than DF.

Focusing on emissions only, the trade-off between CH_4 and NO_X emissions is of the highest importance. Considering that the combustion chamber is not optimised for NG, the acceptable level of methane slip is usually at the level of 10 g/kWh [56]. This is met at boost pressures below 140 kPa ($\lambda < 2.3$) for DF-NG-85. In contrast, NO_X emissions (Fig. 16) drop below the 1 g/kWh threshold at boost pressures above 140 kPa. Replacing DF with HVO at the same energy share halves CH_4 emissions, but is accompanied by nearly a three-fold increase in NO_X emissions. The main reason for this is the aforementioned earlier CA50, resulting in higher peak pressures and temperatures.

Focusing on CoV in IMEP, Fig. 17 shows that cyclic variability keeps at a constant level, below 3 %, for low MAP values. Here one can further see the cause to effect chain explained in the earlier chapter. The increased dilution moves the phasing towards the expansion, and both factors tend towards incomplete combustion, which triggers the residually-affected variability, as with the SOI sweep.

Comparing these CoV results with those from previous fuelling sensitivity section (Fig. 7), one can see that variability in IMEP is lower in Fig. 17, despite air dilution causing higher unburned hydrocarbon emissions than retarded injection. Higher MAP effectively supresses the ratio of retained residuals, which explains the lower sensitivity. Finally, considering the limits of stable combustion, the highly reactive HVO-NG-85 fuel mixture proves to be much more tolerant than DF to air dilution, and provides the best CH_4/NO_X trade-off with this calibration method.

PM emissions, shown in Fig. 18, are generally very low, as already noted for RCCI in general. As such, we omit detailed discussion of particulates, mentioning only the most important remarks. Particulate mass emissions for HVO-NG-85 are higher, but at low PN, because the shorter auto-ignition delay results in the formation of coarse particles. Conversely, in the case of DF as a high-reactivity fuel, PN rapidly increase for high mixture dilution and delayed combustion. However, the particles become finer, so the increase in PN does not increase mass emission.

3.2.3. Sensitivity to EGR

The clear trade-off between NO_X and CH_4 resulting from the air dilution implies that the MAP calibration method discussed in the previous section does not take full advantage of HVO's higher reactivity. This prompts further investigation of alternative methods of dilution to control combustion phasing.

The EGR sweep was conducted with reference SOI of 40 CAD bTDC and the boost pressure at 140 kPa. The EGR was cooled but its temperature was left uncontrolled, as in a real engine. Due to exhaust flow-dependent heat transfer rate, the EGR temperature varied between 90 °C for the lowest recirculation rates, and 110 °C at the heavy recirculation regime. Correspondingly, the intake temperature changed between 26 °C and 50 °C, influenced by the enthalpy balance in the intake

manifold. This should be noted when analysing these EGR sweep outcomes for both DF-NG-85 and HVO-NG-85, synthetically captured in Figs. 19-22.

The combustion timing (Fig. 19) and CoV in IMEP (Fig. 20) results corroborate findings from other parameter sweeps. They indicate that combustion stability can be maintained at higher EGR rates when using HVO instead of DF as high-reactivity fuel. Notably, the HVO-NG-85 mixture exhibits better stability than DF-NG-85 at the same CA50. Therefore, HVO allows higher EGR rates without compromising combustion stability or thermodynamic efficiency.

It implies the CH_4 and NO_X emission trade-off, shown in Figs. 21 and 22. For low EGR, the HVO mixture produces twice as much NO_X as the DF mixture when comparing points with similar CH_4 emissions. This is a direct result of earlier CA50 with the HVO mixture. However, at high EGR, overall emissions are lower for the HVO-NG-85 mixture. Specifically, at operating points with the same CA50 of 371 CAD, HVO-NG-85 with 21 % EGR produces 14 g/kWh CH_4 and 0.21 g/kWh NO_X, while the DF-NG-85 mixture at the same combustion timing produces 24 g/kWh CH_4 and nearly the same amount of NO_X (0.2 g/kWh). This result confirms that at the same BR, with similar mixture distribution (due to the same HRF SOI) and combustion timing, NO_X emissions are independent of the HRF. However, using HVO instead of DF significantly reduces methane slip while maintaining the desired combustion stability. At the same time, the examined range of the EGR sweep practically did not affect PM emissions, which were kept at the reference level for both fuel configurations.

4. Conclusions and outlook

The study formulates the following key statements that affirm the state of the art in RCCI combustion with either diesel or HVO as high-reactivity fuels:

- HVO provides diesel-like performance and emissions in CDC, except PM emissions are halved because of its clean paraffinic makeup. HVO's impact on RCCI is more profound. Here, HVO's increased reactivity advances auto-ignition by as much 5 CAD. Suboptimal phasing causes a deterioration in performance when using HVO at reference RCCI settings, and moves the emissions to CDC-like level, but reduced CH_4 emission implies wider calibration boundaries for HVO without hitting misfire limits.
- Adjusting the airpath parameters (boost pressure, EGR ratio) has a phenomenologically similar effect on RCCI as the fuelling parameters, as both serve to adjust mixture dilution. Thus, the effect on NOx and CA50 remain qualitatively the same for SOI and BR. However, increasing boost pressure and EGR further dilute the gas-air mixture, which is not the case for SOI adjustment, so the strategies face an evident trade-off with increasing CH_4 and CO emission.
- Of the airpath parameters, EGR has a slightly more favourable CH_4 $-NO_X$ emission trade-off than does boost pressure. This is because thermal NO_X reactions can be more effectively supressed with lower heat capacity of recirculated gasses. However, the EGR rate must be relatively mild because the residually-affected feedback loop rapidly increases combustion variability in RCCI.

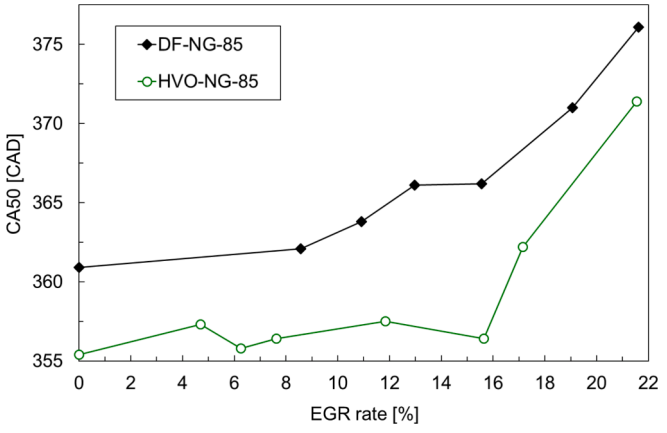

Fig. 19. CA50 for DF and HVO as HRFs, at variable EGR rate.

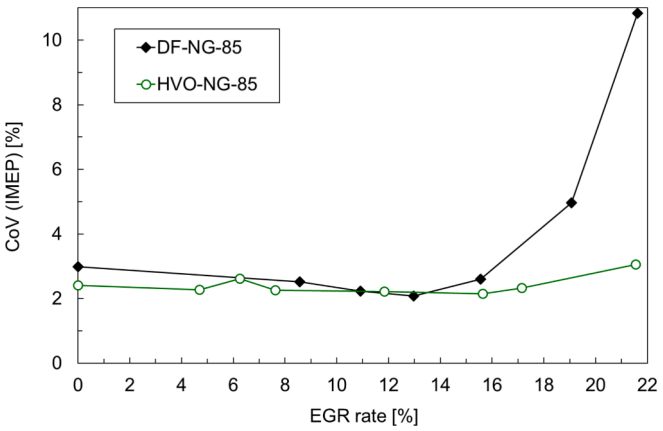

Fig. 20. CoV in IMEP for DF and HVO as HRFs, at variable EGR rate.

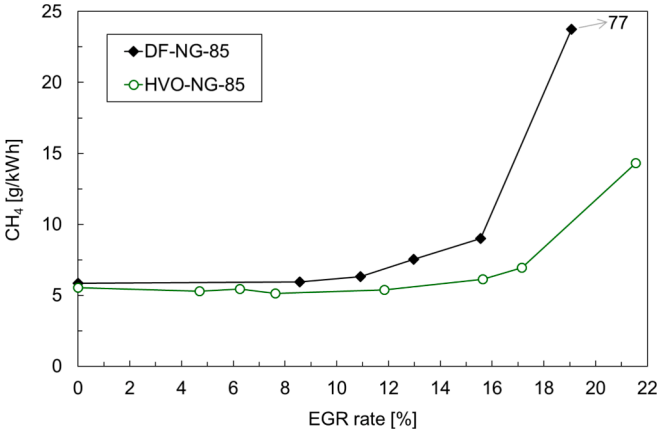

Fig. 21. Emissions of CH_4 for DF and HVO as HRFs, at variable EGR rate.

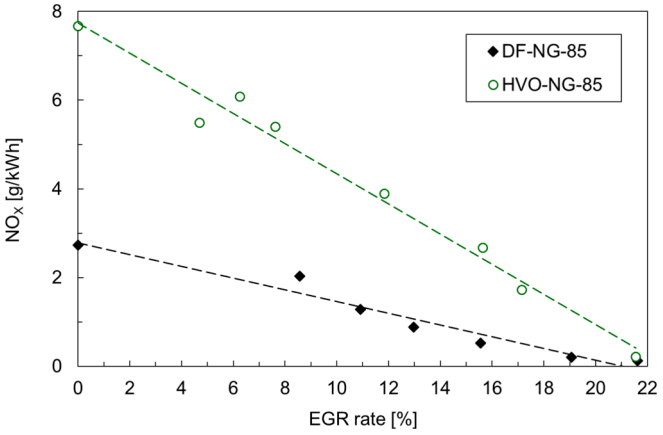

Fig. 22. Emissions of NO_X for DF and HVO as HRFs, at variable EGR rate.

Advancing beyond the current state of the art in combustion phenomenology, the study concludes

- Of the fuelling parameters, the LRF/HRF BR gives greatest RCCI controllability, while SOI provides fine-tuning of the trade-off between combustion phasing and emissions. HVO's response rate to BR adjustment is similar to that typically observed with diesel: adjusting the BR by three percentage points offsets the combustion by 10 CAD. Correspondingly, the response of CA50 to SOI varies from 2:1 CAD to 1:1 CAD.
- When reducing the global (BR ↑) and local (SOI ↑) fuel reactivity, HVO can be better dispersed then diesel, while providing stable and correctly phased combustion. The more uniform dispersion supports better combustion penetration towards the cylinder centreline and reduces local combustion temperature. Methane slip is cut by 50 %, with close to zero NOx emissions.
- Best emissions and performance in RCCI are observed at the boundary of mixture dilution, restricted by the misfire or combustion variability limits. In that sense, no matter the control means, HVO consistently outperforms diesel as it allows greater dilution of the liquid fuel fraction.
- High reactivity (cetane number) plays a decisive role in the above merits achieved by HVO when piloting RCCI. Lower viscosity and density, though supporting better fuel atomisation, appear to have marginal effects with split-injection strategy. The benefits of reduced viscosity and density would be greater if the piston-injection configuration was limited by wall impingement, which was not the case for this setup.

The convolution of the above phenomenological insights enables benchmarking RCCI with HVO and diesel in terms of performance and emission. The applied state-of-the art set by this study narrows down to the following points:

- The best-case DF-NG RCCI yields ultra-high indicated efficiency of 44.8 % and the following emissions: 2.25 g/kWh NO_X; 2.8 g/kWh CO and 9.9 g/kWh CH_4
- Optimised HVO-NGRCCI has the same efficiency (within order of significance) and emissions of: 0.74 g/kWh NO_X; 3.8 g/kWh CO and 5.4 g/kWh CH_4
- Emissions of NO_X and CO, for HVO-activated RCCI, are comfortably within EPA Tier 4 emission limits for non-road mobile machinery. HVO further cuts down methane slip to emission-compliant level without dedicated hardware optimisation. In RCCI, PM results of 0.0015 g/kWh are, from the perspective of contemporary emission norms, negligible.
- For comparison, the state-of-the-art CDC combustion calibration yields 42.7 % thermal efficiency and exceeds EPA Tier 4 standards by approximately 1500 % for NO_X and by nearly 200 % for PM emissions.

This study notes the following limitations and looks towards directions of further research

The study characterised the particulate emission comprehensively in a broad range between CDC and RCCI regime. This comprehensive approach, however, forms a limitation in this case. The ultra-low level of particulates in RCCI and the adopted calibration range render the fuel-to-fuel differences in RCCI mode statistically irrelevant. This is why PM emission and PN results were not discussed in detail. However, some systematics that we have pointed out in the results discussion imply that the mechanisms influencing particulate formation in RCCI mode, considering high-reactivity fuel differences, are not trivial. They deserve a dedicated pre-study of the subject, with tailor-made methods and problem-specific design of experiments. We see this as a relevant research direction on the fundamental side.

The design of experiments adopted in the present study, prioritising individual control-parameter sweeps, supported understanding of the mechanisms responsible for large-scale differences in RCCI performance with HVO. This means that optimum RCCI points reported for HVO and diesel, do not represent the full emission and performance potentials. Further improvement is possible with multi-parameter co-optimisation, supported by a finer focus around the local minima revealed by this study. The follow-up, applied-oriented study, aiming to explicitly quantify the performance of HVO-natural gas RCCI, will be combined with hardware optimisation. This latter aspect will look in particular at reducing the effect of upper crevices in the combustion chamber, valve timing and optimising the compression ratio. With this combination of measures, it is foreseen that HVO-optimised RCCI combustion can surpass the 50 % thermal efficiency threshold, while complying with even stricter emission values than the EPA NRMM Tier 4 limits set as a reference for this study.

CRediT authorship contribution statement

Jacek Hunicz: Writing – review & editing, Writing – original draft, Supervision, Project administration, Methodology, Funding acquisition, Conceptualization. **Liping Yang:** Writing – original draft, Funding acquisition, Conceptualization. **Arkadiusz Rybak:** Visualization, Resources, Investigation, Formal analysis, Data curation. **Shuaizhuang Ji:** Writing – original draft, Formal analysis, Data curation. **Michał S. Gęca:** Software, Resources, Methodology, Investigation. **Maciej Mikulski:** Writing – review & editing, Writing – original draft, Supervision, Investigation, Funding acquisition, Conceptualization.

Declaration of competing interest

The authors declare that they have no known competing financial interests or personal relationships that could have appeared to influence the work reported in this paper.

Acknowledgements

Jacek Hunicz and Liping Yang gratefully acknowledge the Chinese Ministry of Science and Technology for supporting this research through the National Foreign Experts Program (grant No. G2023180006L) and National Natural Science Foundation of China (grant No. 52171298).

The experimental facilities used in this research were provided with support from the commissioned task entitled "VIA CARPATIA Universities of Technology Network named after the President of the Republic of Poland Lech Kaczyński", contract No. MEiN/2022/DPI/2575.

Maciej Mikulski Acknowledges the Flexible Clean Propulsion Technologies project with financial support from Business Finland (ref. 1310/31/2023).

Data availability

Data will be made available on request.

References

[1] Reitz RD, Ogawa H, Payri R, Fansler T, Kokjohn S, Moriyoshi Y, et al. IJER editorial: the future of the internal combustion engine. Int J Engine Res 2020;21:3–10. https://doi.org/10.1177/1468087419877990.
[2] Agarwal AK, Singh AP, García A, Monsalve-Serrano J. Challenges and opportunities for application of reactivity-controlled compression ignition combustion in commercially viable transport engines. Prog Energy Combust Sci 2022;93:101028. https://doi.org/10.1016/J.PECS.2022.101028.
[3] Kokjohn S, Hanson R, Splitter D, Kaddatz J, Reitz R. Fuel Reactivity Controlled Compression Ignition (RCCI) combustion in light- and heavy-duty engines. SAE Int J Engines 2011;4:360–74. https://doi.org/10.4271/2011-01-0357.
[4] Dryer FL. Chemical kinetic and combustion characteristics of transportation fuels. Proc Combust Inst 2015;35:117–44. https://doi.org/10.1016/J.PROCI.2014.09.008.
[5] Kokjohn SL, Reitz RD. Reactivity controlled compression ignition and conventional diesel combustion: a comparison of methods to meet light-duty NOx and fuel

economy targets. Int J Engine Res 2013;14:452–68. https://doi.org/10.1177/1468087413476032.
[6] Paykani A, Garcia A, Shahbakhti M, Rahnama P, Reitz RD. Reactivity controlled compression ignition engine: Pathways towards commercial viability. Appl Energy 2021;282:116174. https://doi.org/10.1016/J.APENERGY.2020.116174.
[7] Kokjohn SL, Musculus MPB, Reitz RD. Evaluating temperature and fuel stratification for heat-release rate control in a reactivity-controlled compression-ignition engine using optical diagnostics and chemical kinetics modeling. Combust Flame 2015;162:2729–42. https://doi.org/10.1016/J.COMBUSTFLAME.2015.04.009.
[8] Yousefi A, Guo H, Birouk M. Effect of swirl ratio on NG/diesel dual-fuel combustion at low to high engine load conditions. Appl Energy 2018;229:375–88. https://doi.org/10.1016/J.APENERGY.2018.08.017.
[9] Reitz RD, Duraisamy G. Review of high efficiency and clean reactivity controlled compression ignition (RCCI) combustion in internal combustion engines. Prog Energy Combust Sci 2015;46:12–71. https://doi.org/10.1016/J.PECS.2014.05.003.
[10] Gürsan C, de Gooyert V. The systemic impact of a transition fuel: does natural gas help or hinder the energy transition? Renew Sustain Energy Rev 2021;138:110552. https://doi.org/10.1016/J.RSER.2020.110552.
[11] Nieman DE, Dempsey AB, Reitz RD. Heavy-duty RCCI operation using natural gas and diesel. SAE Int J Engines 2012;5:270–85. https://doi.org/10.4271/2012-01-0379.
[12] Dronniou N, Kashdan J, Lecointe B, Sauve K, Soleri D. Optical investigation of dual-fuel CNG/diesel combustion strategies to reduce CO2 emissions. SAE Int J Engines 2014;7:873–87. https://doi.org/10.4271/2014-01-1313.
[13] Li Y, Li H, Guo H, Li Y, Yao M. A numerical investigation on methane combustion and emissions from a natural gas-diesel dual fuel engine using CFD model. Appl Energy 2017;205:153–62. https://doi.org/10.1016/j.apenergy.2017.07.071.
[14] Yang L, Ji S, Niu W, Zare A, Hunicz J, Brown RJ. Effect of split injection strategy of diesel fuel on multi-stage heat release and performance of a RCCI engine fueled with diesel and natural gas. Fuel 2024;362:130930. https://doi.org/10.1016/J.FUEL.2024.130930.
[15] Doosje E, Willems F, Baert R. Experimental demonstration of RCCI in heavy-duty engines using diesel and natural gas. SAE Tech Pap 2014;1. https://doi.org/10.4271/2014-01-1318.
[16] Mikulski M, Bekdemir C. Understanding the role of low reactivity fuel stratification in a dual fuel RCCI engine – a simulation study. Appl Energy 2017;191:689–708. https://doi.org/10.1016/J.APENERGY.2017.01.080.
[17] Xu G, Jia M, Li Y, Chang Y, Liu H, Wang T. Evaluation of variable compression ratio (VCR) and variable valve timing (VVT) strategies in a heavy-duty diesel engine with reactivity controlled compression ignition (RCCI) combustion under a wide load range. Fuel 2019;253:114–28. https://doi.org/10.1016/J.FUEL.2019.05.020.
[18] Mikulski M, Balakrishnan PR, Doosje E, Bekdemir C. Variable valve actuation strategies for better efficiency load range and thermal management in an RCCI engine. SAE Tech Pap. 2018. https://doi.org/10.4271/2018-01-0254.
[19] Motallebi Hasankola SS, Shafaghat R, Jahanian O, Talesh Amiri S, Shooghi M. Numerical investigation of the effects of inlet valve closing temperature and exhaust gas recirculation on the performance and emissions of an RCCI engine. J Therm Anal Calorim 2020;139:2465–74. https://doi.org/10.1007/S10973-019-08513-0/METRICS.
[20] Huang F, Li L, Zhou M, Wan M, Shen L, Lei J. Effect of EGR on performance and emissions of a methanol–diesel reactivity controlled compression ignition (RCCI) engine. J Brazilian Soc Mech Sci Eng 2023;45:1–12. https://doi.org/10.1007/S40430-023-04289-5/METRICS.
[21] Mikulski M, Balakrishnan PR, Hunicz J. Natural gas-diesel reactivity controlled compression ignition with negative valve overlap and in-cylinder fuel reforming. Appl Energy 2019;254:113638. https://doi.org/10.1016/J.APENERGY.2019.113638.
[22] Kim J, Soleimani A, Nousiainen P, Axelsson M, Mikulski M. Variable valve actuation for next generation marine and off-road engines - a comprehensive review oriented on meeting future emission legislation. SSRN Electron J 2024. https://doi.org/10.2139/SSRN.4760136.
[23] Zhang Y, Matthias V, Liu H, Moldanova J, Moussiopoulos N, Lehtoranta K, et al. Methane emissions from a state-of-the-art LNG-powered vessel. Atmos. 2023;14:825. https://doi.org/10.3390/ATMOS14050825.
[24] Vasudev A, Mikulski M, Balakrishnan PR, Storm X, Hunicz J. Thermo-kinetic multi-zone modelling of low temperature combustion engines. Prog Energy Combust Sci 2022;91:100998. https://doi.org/10.1016/J.PECS.2022.100998.
[25] Varuvel EG, Seetharaman S, Joseph Shobana Bai FJ, Devarajan Y, Balasubramanian D. Development of artificial neural network and response surface methodology model to optimize the engine parameters of rubber seed oil – hydrogen on PCCI operation. Energy 2023;283:129110. https://doi.org/10.1016/J.ENERGY.2023.129110.
[26] Singh S, Rao DG, Dixit M. Experimental investigation of a reactivity controlled compression ignition engine fuelled with liquified petroleum gas. Univers J Mech Eng 2023;11:25–35. https://doi.org/10.13189/UJME.2023.110201.
[27] Li Y, Jia M, Liu Y, Xie M. Numerical study on the combustion and emission characteristics of a methanol/diesel reactivity controlled compression ignition (RCCI) engine. Appl Energy 2013;106:184–97. https://doi.org/10.1016/J.APENERGY.2013.01.058.
[28] Fakhari AH, Gharehghani A, Salahi MM, Mahmoudzadeh Andwari A, Mikulski M, Hunicz J, et al. Numerical investigation of ammonia-diesel fuelled engine operated in RCCI mode. SAE Tech Pap 2023. https://doi.org/10.4271/2023-24-0057.
[29] Fakhari AH, Gharehghani A, Salahi MM, Andwari AM. Numerical investigation of the hydrogen-enriched ammonia-diesel RCCI combustion engine. Fuel 2024;375:132579. https://doi.org/10.1016/J.FUEL.2024.132579.
[30] Vasudev A, Mikulski M, Hyvönen J. Effects of H2 admixture on RCCI combustion dual-fuel marine engines: a model-based study - Clean Propulsion. IEEES 2023 – Proc B 2023;2023:61–5.
[31] Hanson R, Curran S, Wagner R, Reitz RD, Hanson R, Curran S, et al. Effects of biofuel blends on RCCI combustion in a light-duty, multi-cylinder diesel engine. SAE Int J Engines 2013;6:488–503. https://doi.org/10.4271/2013-01-1653.
[32] García A, Monsalve-Serrano J, Villalta D, Lago Sari R, Gordillo Zavaleta V, Gaillard P. Potential of e-Fischer Tropsch diesel and oxymethyl-ether (OMEx) as fuels for the dual-mode dual-fuel concept. Appl Energy 2019;253. https://doi.org/10.1016/j.apenergy.2019.113622.
[33] Duraisamy G, Rangasamy M, Govindan N. A comparative study on methanol/diesel and methanol/PODE dual fuel RCCI combustion in an automotive diesel engine. Renew Energy 2020;145:542–56. https://doi.org/10.1016/j.renene.2019.06.044.
[34] Pinto GM, da Costa RBR, de Souza TAZ, Rosa AJAC, Raats OO, Roque LFA, et al. Experimental investigation of performance and emissions of a CI engine operating with HVO and farnesane in dual-fuel mode with natural gas and biogas. Energy 2023;277:127648. https://doi.org/10.1016/J.ENERGY.2023.127648.
[35] Rimkus A, Stravinskas S, Matijošius J, Hunicz J. Effects of different gas energy shares on combustion and emission characteristics of compression ignition engine fueled with dual-fossil fuel and dual-biofuel. Energy 2024;312:133443. https://doi.org/10.1016/J.ENERGY.2024.133443.
[36] Sun W, Zeng W, Guo L, Zhang H, Yan Y, Lin S, et al. Experimental investigation into the effects of pilot fuel and intake condition on combustion and emission characteristics of RCCI engine. Fuel 2022;325:124912. https://doi.org/10.1016/J.FUEL.2022.124912.
[37] Gowthama Krishnan M, Rajkumar S, Devarajan Y, Rajiv A. A comprehensive review on advancement and challenges of renewable biofueled reactivity controlled compression ignition (RCCI) engine. J Energy Inst 2024;113:101540. https://doi.org/10.1016/J.JOEI.2024.101540.
[38] Flach B, Lieberz S, Bolla S. EU Biofuels Annual 2019 - Reports GAIN Report Number: NL9022 n.d. https://www.etipbioenergy.eu/databases/reports/429-eu-biofuels-annual-2019 (accessed August 5, 2024).
[39] Vásquez MC, Silva EE, Castillo EF. Hydrotreatment of vegetable oils: a review of the technologies and its developments for jet biofuel production. Biomass Bioenergy 2017;105:197–206. https://doi.org/10.1016/J.BIOMBIOE.2017.07.008.
[40] Sasaki S, Kato M, Yokota T, Konno M, Gill D. An experimental study of injection and combustion with dimethyl ether. SAE Tech Pap. 2015. https://doi.org/10.4271/2015-01-0932.
[41] Hunicz J, Matijošius J, Rimkus A, Kilikevičius A, Kordos P, Mikulski M. Efficient hydrotreated vegetable oil combustion under partially premixed conditions with heavy exhaust gas recirculation. Fuel 2020;268:117350. https://doi.org/10.1016/J.FUEL.2020.117350.
[42] Hunicz J, Mikulski M, Shukla PC, Gęca MS. Partially premixed combustion of hydrotreated vegetable oil in a diesel engine: sensitivity to boost and exhaust gas recirculation. Fuel 2022;307:121910. https://doi.org/10.1016/J.FUEL.2021.121910.
[43] Žvar Baškovič U, Vihar R, Rodman Oprešnik S, Seljak T, Katrašnik T. RCCI combustion with renewable fuel mix – tailoring operating parameters to minimize exhaust emissions. Fuel 2022;311. https://doi.org/10.1016/J.FUEL.2021.122590.
[44] Cheng Q, Tuomo H, Kaario OT, Martti L. Spray dynamics of HVO and EN590 diesel fuels. Fuel 2019;245:198–211. https://doi.org/10.1016/J.FUEL.2019.01.123.
[45] Hulkkonen T, Hillamo H, Sarjovaara T, Larmi M. Experimental study of spray characteristics between hydrotreated vegetable oil (HVO) and crude oil based EN 590 diesel fuel. SAE Tech Pap 2011. https://doi.org/10.4271/2011-24-0042.
[46] Wu L, Liu Y. Environmental impacts of hydrotreating processes for the production of clean fuels based on life cycle assessment. Fuel 2016;164:352–60. https://doi.org/10.1016/J.FUEL.2015.10.017.
[47] Millo F, Rafigh M, Andreata M, Vlachos T, Arya P, Miceli P. Impact of high sulfur fuel and de-sulfation process on a close-coupled diesel oxidation catalyst and diesel particulate filter. Fuel 2017;198:58–67. https://doi.org/10.1016/J.FUEL.2017.01.006.
[48] Suarez-Bertoa R, Kousoulidou M, Clairotte M, Giechaskiel B, Nuottimäki J, Sarjovaara T, et al. Impact of HVO blends on modern diesel passenger cars emissions during real world operation. Fuel 2019;235:1427–35. https://doi.org/10.1016/J.FUEL.2018.08.031.
[49] Maurya RK. Estimation of optimum number of cycles for combustion analysis using measured in-cylinder pressure signal in conventional CI engine. Measurement 2016;94:19–25. https://doi.org/10.1016/J.MEASUREMENT.2016.07.065.
[50] Siadkowska K, Barański G. Combustion stability for early and late direct hydrogen injection in a dual fuel diesel engine. Combust Engines 2024;196:89–98. https://doi.org/10.19206/CE-171390.
[51] Heywood JB. Internal Combustion Engine Fundamentals 2018.
[52] Martyr AJ, Plint MA. Engine testing: the design, building, modification and use of powertrain test facilities. Fourth Edition Elsevier 2012. https://doi.org/10.1016/C2010-0-66322-X.
[53] Hohenberg GF. Advanced approaches for heat transfer calculations. SAE Tech Pap 1979. https://doi.org/10.4271/790825.
[54] Mikulski M, Vasudev A, Hunicz J, Rybak A, Gęca M. Combustion of hydrotreated vegetable oil in a diesel engine: sensitivity to split injection strategy and exhaust gas recirculation. In: ASME 2020 Intern Combust Engine Div Fall Tech Conf ICEF; 2021. https://doi.org/10.1115/ICEF2020-2936.

[55] Hunicz J, Mikulski M, Shukla PC, Gęca MS. Partially premixed combustion of hydrotreated vegetable oil in a diesel engine: Sensitivity to boost and exhaust gas recirculation. Fuel 2022;307. https://doi.org/10.1016/J.FUEL.2021.121910.
[56] Alkidas AC. Combustion-chamber crevices: the major source of engine-out hydrocarbon emissions under fully warmed conditions. Prog Energy Combust Sci 1999;25:253–73. https://doi.org/10.1016/S0360-1285(98)00026-4.
[57] Hunicz J, Mikulski M, Koszałka G, Ignaciuk P. Detailed analysis of combustion stability in a spark-assisted compression ignition engine under nearly stoichiometric and heavy EGR conditions. Appl Energy 2020;280:115955. https://doi.org/10.1016/J.APENERGY.2020.115955.
[58] CARB provides an update on Tier 5 emission standards for off-road engines n.d. https://dieselnet.com/news/2023/11carb.php (accessed November 2, 2024).